Antimicrobial and Antibiofilm Properties of Fluorinated Polymers with Embedded Functionalized Nanodiamonds

Nunes-Pereira, João; Costa, Pedro; Fernandes, Liliana; Carvalho, Estela O.; Fernandes, Margarida M.; Carabineiro, Sónia A.C.; Buijnsters, Josephus G.; Tubio, Carmen R.; Lanceros-Mendez, Senentxu

DOI
10.1021/acsapm.0c00869

Publication date
2020

Document Version
Final published version

Published in
ACS Applied Polymer Materials

Citation (APA)
Nunes-Pereira, J., Costa, P., Fernandes, L., Carvalho, E. O., Fernandes, M. M., Carabineiro, S. A. C., Buijnsters, J. G., Tubio, C. R., & Lanceros-Mendez, S. (2020). Antimicrobial and Antibiofilm Properties of Fluorinated Polymers with Embedded Functionalized Nanodiamonds. *ACS Applied Polymer Materials*, *2*(11), 5014-5024. https://doi.org/10.1021/acsapm.0c00869

ACS APPLIED POLYMER MATERIALS

pubs.acs.org/acsapm Article

Antimicrobial and Antibiofilm Properties of Fluorinated Polymers with Embedded Functionalized Nanodiamonds

João Nunes-Pereira,* Pedro Costa, Liliana Fernandes, Estela O. Carvalho, Margarida M. Fernandes, Sónia A. C. Carabineiro, Josephus G. Buijnsters, Carmen R. Tubio, and Senentxu Lanceros-Mendez*

Cite This: *ACS Appl. Polym. Mater.* 2020, 2, 5014−5024 Read Online

ACCESS | Metrics & More | Article Recommendations | Supporting Information

ABSTRACT: Environmentally resilient antimicrobial coatings are becoming increasingly required for a wide range of applications. For this purpose, nanocomposite thin films of poly(vinylidene fluoride) (PVDF) filled with several types of functionalized nanodiamonds (NDs) were processed by solvent casting. The effects of ND inclusion and functionalization in their morphological, structural, optical, thermal, and electrical properties were evaluated taking into account the type of the nanofiller and a concentration up to 2 wt %. The morphology, structure, and thermal features of the polymer matrix are governed by the processing conditions, and no noticeable changes occurred due to the presence of the ND fillers. The polymer crystallized mainly in the α phase with a crystallinity of ≈60%. In turn, the optical transmittance from 200 to 800 nm and the dielectric constant effectively depended on the ND type and content. The inclusion of the ND particles effectively provided antimicrobial properties to the films, which depended on the ND functionalization. This study thus shows that the incorporation of functionalized NDs into PVDF allows the development of antimicrobial coatings with tailorable optical and dielectric properties, which could be of great importance to face nowadays pandemic crisis scenario.

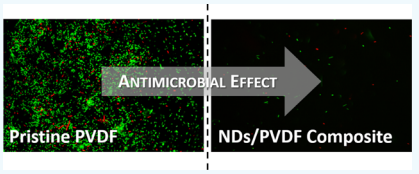

KEYWORDS: *nanodiamonds, poly(vinylidene fluoride), solvent casting, polymer composites, antimicrobial films*

INTRODUCTION

Polymer composite science and technology is a rapidly increasing field of research, mostly due to the possibilities on tailoring material functional properties for application in a large variety of areas. The introduction of small amounts of a nanomaterial within a polymeric matrix can lead to large enhancements to its features, such as optical, mechanical, electrical, and thermal properties.[1,2] Furthermore, new functional properties can be added otherwise not existing in the polymer matrix, such as magnetic[3] or photochromic[4] response, among others. Other properties that can be added and/or enhanced are those related to the applicability of the materials as coatings, such as tailored hydrophobicity,[5] self-cleaning,[6] or antimicrobial features.[7]

Among the many nanomaterials synthetized in recent years, nanocarbons have been intensively used for several purposes. In particular, diamond nanostructures (nanodiamonds, NDs) were synthesized for the first time in the 1960s and remained practically unexplored until the 1990s when important breakthroughs led to an increasing interest in the applications of these nanostructures. NDs present enhanced mechanical properties (including Young's modulus and hardness), elevated electrical resistivity and thermal conductivity (up to about 2000 W/m·K), high surface area with tunable surface structure, and optical properties such as photoluminescence (nitrogen-vacancy centers). Further, they are biocompatible, chemically stable, and resistant to severe environment conditions and offer the possibility to attach different functional groups to their surface without losing the main features of the diamond core.[8−10] Thus, the aforementioned properties along with the rich chemistry of the surface make NDs excellent nanostructures for developing polymer composites, and nowadays, NDs are being explored for a large number of applications, such as drug delivery, cancer therapy, biosensors, surgical implants, tissue engineering, biomedical imaging, tribology and lubrication, and antimicrobial applications.[8,11,12] Yet, other materials composed by nanostructures of carbon, e.g., carbon nanotubes, fullerene, diamond-like carbon, and graphene demonstrated to have a wide spectrum of antibacterial activities for different pathogens.[13] As such, they have been investigated as fillers in polymeric matrices for developing materials displaying antifouling, antibiofilm, and antimicrobial properties[14] in a similar approach to other antimicrobial materials comprising nanostructures. Standard antibacterial coatings or surfaces are usually produced by incorporating antimicrobial agents, such as copper and copper alloys,[15] silver compounds,[16] or organic molecules containing quaternary ammonium chemical groups.[17] However, concerns about the cytotoxicity of these nanoparticles against human cells have been expressed.[18,19]

Received: August 10, 2020
Accepted: September 29, 2020
Published: September 29, 2020

https://dx.doi.org/10.1021/acsapm.0c00869
ACS Appl. Polym. Mater. 2020, 2, 5014−5024

Due to their biocompatibility, tailorable surface chemistry and large surface area, NDs have already been studied for nontoxic antimicrobial/antifungal materials[20] as well as for other applications like adsorption and controlled release of anticancer drugs, such as 4-hydroxytamoxifen,[21] paclitaxel,[22] and tetracyclines.[23,24] Combining the attachment of specific drugs to the ND surface with controlled release provides a new opportunity for anticancer chemotherapeutics. Its elevated hardness, Young's modulus, rich chemistry of the surface, and chemical properties make the core of NDs suitable to enhance the mechanical and chemical properties of bioresorbable polymer scaffolds for tissue engineering, as demonstrated in PLGA (poly(lactic-*co*-glycolic acid)) filled with phospholipid ND compound (NDPC), which has been successfully evaluated for bone tissue engineering *in vivo* and *in vitro*.[25] ND particles are also stable in aqueous media, making them suitable to use in the design of modified electrodes and a promising material for electrochemical sensors with high analytical performance.[26]

With the introduction of NDs to polymeric matrices, the composites obtained have superior thermal, mechanical, and optical properties that, combined with the biocompatibility and chemical stability of the NDs, provide important options for biomedical applications.[8,27] Among the broad range of polymer matrices able to be combined with ND fillers, PVDF (poly(vinylidene fluoride)) and copolymers are an attractive choice in the case of multifunctional polymer coatings due to their remarkable electroactive characteristics, namely, pyro-, piezo-, and ferroelectric effects, which makes them a suitable choice to develop advanced and functional materials, including sensors and actuators.[12,28] PVDF can crystallize in five distinct phases, α, β, and γ being the most common. This polymer has some outstanding features such as high chemical and UV resistances, mechanical strength, hydrophobicity, thermal stability, and flexibility compared to several commercial polymeric materials, which drives the manufacture of new PVDF-based nanocomposites for technological applications.[28,29] The electroactive properties of PVDF have been used to develop new strategies for tailoring bacterial behavior, either growth or inhibition of *Staphylococcus epidermidis* and *Escherichia coli*, mainly when mechanically stimulated.[30] This study reports the production of ND/PVDF composites by solvent casting. It is worth noting that solvent casting approaches are gaining increasing interest as they allow processing by additive manufacturing fabrication processes, such as spray, screen, or even ink-jet printing,[31] suitable for the implementation of coatings and devices. The morphology, structural, optical, thermal, and electrical properties of the ND/PVDF composite films were evaluated as well as their antimicrobial characteristics, which proved to be suitable to develop antiseptic materials of high interest to deal with pandemic crises in order to avoid bacterial co-infections. In fact, serious secondary bacterial infections are considered an important complication of SARS-CoV-2 virus infection (COVID-19).[32]

EXPERIMENTAL DETAILS

Materials. PVDF (Solef 1010) was obtained from Solvay. DMF (*N*,*N*-dimethylformamide, 99.5%) solvent was acquired from Fluka. uDiamond Molto (non-functionalized ND, hereafter denoted as NDM), with 5 nm average particle size, was obtained from Carbodeon Ltd. Oy, Vantaa (Finland). Functionalized samples, namely, uDiamond Vox P (carboxyl monofunctionalized, hereafter denoted as NDO), uDiamond Amine P (amine monofunctionalized, hereafter denoted as NDA), and uDiamond Hydrogen P (hydrogen monofunctionalized, hereafter denoted as NDH), were also obtained from the same supplier.

Sample Preparation. The ND/PVDF-based composites followed a typical solvent casting method using the doctor blade technique.[29] Initially, the ND particles were dispersed in DMF and placed in an ultrasound bath for 4 h. The PVDF powder was added to the solution at a ratio of 10/90 wt % of PVDF/DMF, and the relative concentration of the ND fillers to polymer varied between 0.25 and 2 wt %. The solution was magnetically stirred at 40 °C, until the PVDF sample completely dissolved, and then spread with a bar coater on top of a clean glass substrate. Solvent evaporation was performed at 210 °C (above the melting temperature of PVDF) in an oven (Binder, ED23) to obtain composite films with a thickness of 20−25 μm and a compact morphology to evaluate the effect of nanofillers−polymer interactions in the crystallization of the composites as these processing conditions lead to preferential crystallization in the α phase of PVDF.[29] Hereafter, the polymer composites will be identified by the ND nanoparticles functionalization type (NDM, NDA, NDO, and NDH, respectively) and the respective nanofiller amount (in wt %).

Sample Characterization. Surface element quantification of the ND/PVDF composites was carried out by X-ray photoelectron spectroscopy (XPS, Kratos AXIS Ultra HSA spectrometer). A monochromatic Al Kα X-ray source (1486.7 eV) was used in fixed analyzer transmission (FAT) mode at 15 kV (90 W), with 40 eV of pass energy for regions ROI and a survey of 80 eV. A charge neutralization system was used to acquire data at a pressure of $<1 \times 10^{-6}$ Pa. Survey and multiregion spectra were obtained for C1s, O1s, and N1s peaks, and the values of binding energy were referred to the C1s peak at 284.6 eV. The obtained spectra were fitted to Gaussian and Lorentzian curves with CASA XPS software after a Shirley background subtraction.

The nanoparticles distribution and composites morphology were analyzed by SEM (scanning electron microscopy, NanoSEM - FEI Nova 200 (FEG/SEM)), with 15 kV of accelerating voltage. Prior evaluation, a thin layer of gold (20 nm) was deposited on the samples by magnetron sputtering (Polaron SC502).

AFM (atomic force microscopy, CSInstruments setup) was performed to study the surface roughness of the samples. Measurements were performed in squares of 20 × 20 μm^2 in the non-contact resonant mode (73 kHz of frequency and 84° of amplitude) to avoid samples damage and AFM tangling.

The surface wettability was studied by contact angle measured in a Dataphysics system OCA20 at room temperature with ultrapure water (5 μL) in different spots for each sample. The SCA20 software allowed one to determine the contact angle, and the results are presented as an average of six measurements per sample with the respective standard deviation (SD).

The UV−Vis spectroscopy experiments (Jasco V-670 spectrophotometer) were performed at room temperature to study the optical characteristics of the composites, within the range of 200−900 nm.

Fourier transform infrared spectroscopy (FTIR) in attenuated total reflectance (ATR) mode (Jasco FT/IR-4100) was performed to study the polymer phase in the composites. Thirty-two scans with a resolution of 4 cm^{-1} were carried out in the range of 4000−600 cm^{-1}. Considering that the polymer crystallizes mainly in the α or β phases, the α-PVDF relative content ($F(\alpha)$) was calculated considering the absorbance at 766 cm^{-1} (A_α) and 840 cm^{-1} (A_β) and the absorption coefficients at the correspondent wavenumber ($K_\alpha = 6.1 \times 10^4$ $cm^2 \cdot mol^{-1}$; $K_\beta = 7.7 \times 10^4$ $cm^2 \cdot mol^{-1}$) after eq 1:[28]

$$F(\alpha) = \frac{A_\alpha}{\left(\frac{K_\alpha}{K_\beta}\right)A_\beta + A_\alpha} \quad (1)$$

The thermal properties of the composites were analyzed by DSC (differential scanning calorimetry) thermography (Perkin-Elmer DSC 8000). The measurements were performed at a heating rate of 10 °C/min, under a flowing nitrogen atmosphere, in the range of 25−250

https://dx.doi.org/10.1021/acsapm.0c00869
ACS Appl. Polym. Mater. 2020, 2, 5014−5024

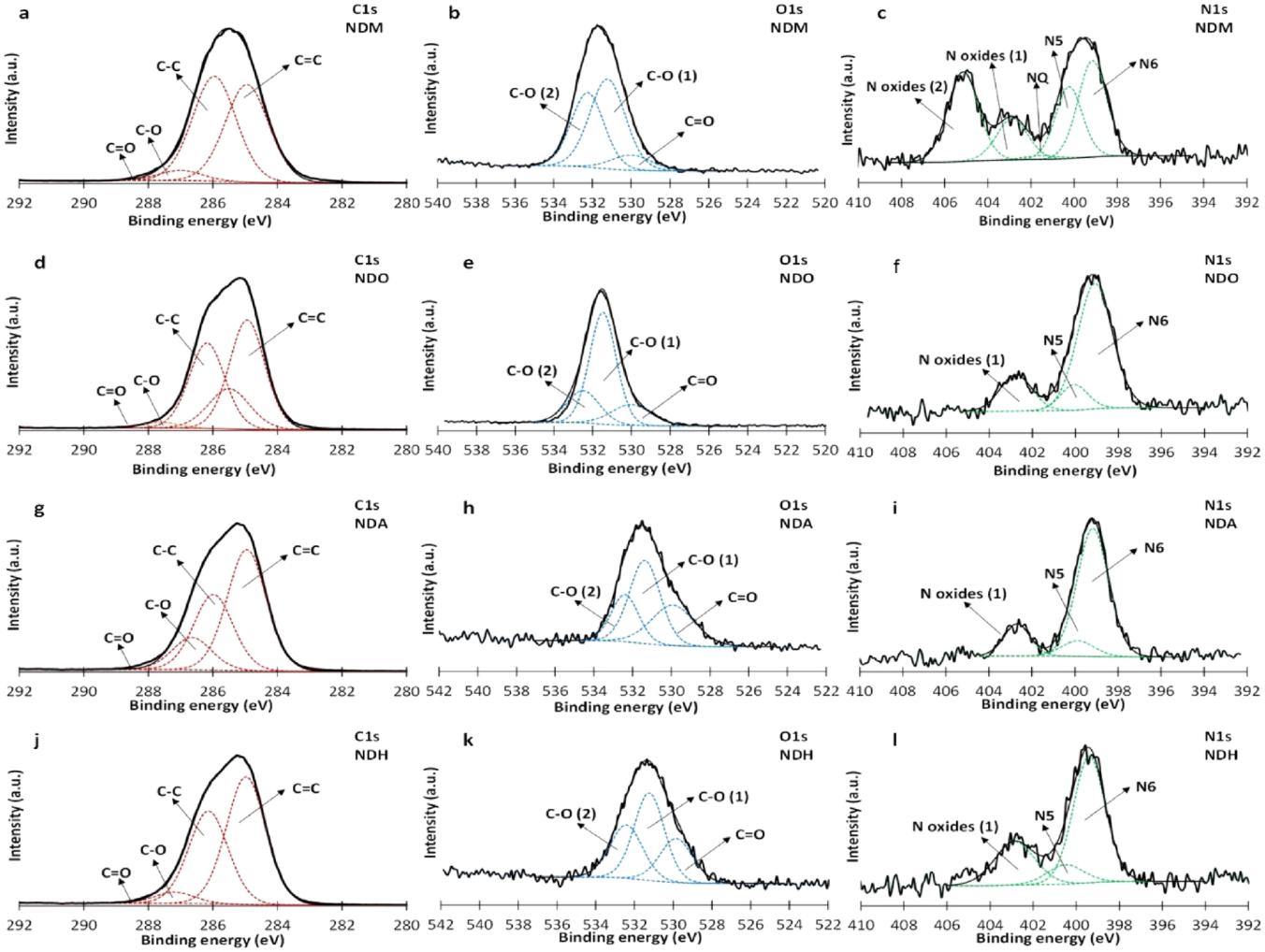

Figure 1. XPS spectra and deconvolution of C1s (a, d, g, j), O1s (b, e, h, k), and N1s (c, f, i, l) regions of the different ND samples: NDM (a–c), NDO (d–f), NDA (g–i), and NDH (j–l).

°C. 30 μL perforated aluminum pans were used to release volatiles. The degree of crystallinity (χ_c) was determined by the melting enthalpy of the sample (ΔH_f) and the melting enthalpy of PVDF 100% crystalline (ΔH_{100}, 104.6 J/g) through eq 2:[33]

$$\chi_c = \frac{\Delta H_f}{\Delta H_{100}} \tag{2}$$

Prior to the electrical characterization circular gold electrodes (5 mm diameter) were deposited on both film sides by sputtering (Polaron SC502 sputter coater) under the following conditions: 3 × 30 s at ≈20 mbar and ≈20 mA.

The dielectric analysis was performed measuring the capacity (C) and the dielectric loss ($\tan(\delta)$) at room temperature with a LCR meter (Quadtech 1920) applying a signal voltage of 1.0 V sweeping the frequency from 500 Hz to 1 MHz. To calculate the dielectric constant (ε') the geometrical parameters (error of ≈1%) of the parallel plate capacitor were considered.

The a.c. conductivity (σ') was calculated from dielectric measurements through the angular frequency (ω), the permittivity of the free space (ε_0), and the imaginary part of ε' dependent of frequency (ε'') by eq 3:

$$\sigma' = \omega \varepsilon_0 \varepsilon'' \tag{3}$$

The d.c. electrical conductivity (σ) was determined after obtaining the d.c. volumetric electrical resistivity (ρ_v) from the characteristic IV curves obtained with a picoammeter/voltage source (Keithley 487) through the electrical resistance (R), sample thickness (L), and electrode area (A) by eq 4:

$$\frac{1}{\sigma} = \rho_v = R\frac{L}{A} \tag{4}$$

Antimicrobial and Antibiofilm Activity. The inhibition of bacterial growth was assessed against a Gram-negative, *Escherichia coli* (*E. coli*) strain ATCC 8739 acquired from the American Type Culture Collection (LGC Standards S.L.U, Spain). To prepare the bacterial inoculum, a single colony was isolated from an agar plate and grown in Nutrient Broth (NB, Dehydrated Culture Media, Panreac) overnight, at 37 °C and 110 rpm, until the stationary phase was reached. The bacterial cell population was estimated using spectrophotometer optical density (OD) readings at 600 nm and adjusted as required in each experiment. This process was performed for all bacterial assays.

Nanodiamond Bacteriostatic Activity. Bacterial susceptibility to the non-functionalized and different functionalized NDs was measured in suspension through a microdilution assay performed in NB. Succinctly, various concentrations of ND working solutions were prepared by performing 10-fold serial dilutions of a starting solution of 0.16 mg·mL^{-1}. A 96-well polystyrene plate was filled with 75 μL of ND diluted solutions and 75 μL of bacterial inoculum, obtaining the final concentration of 5 × 10^5 CFU (colony-forming units) mL^{-1}. The bacterial growth was assessed after 24 h through OD measurements at 600 nm with a microplate reader (Biotek Cytation3). The reported

https://dx.doi.org/10.1021/acsapm.0c00869
ACS Appl. Polym. Mater. 2020, 2, 5014–5024

growth inhibition rates were the mean values of four independent experiments with the respective SD.

Film Bacteriostatic Activity. *E. coli* bacteriostatic activity assessed in contact with the processed ND/PVDF composite films was evaluated. First, the films were cut into disks of 13 mm in diameter, sterilized, and placed on 24-well nontreated polystyrene plates. A bacterial inoculum of 5×10^5 CFU·mL^{-1} was incubated overnight at a temperature of 37 °C. The bacterial cultures were further diluted in phosphate buffer solution (PBS) and plated (100 μL) on a NB agar plate and incubated at 37 °C. After 24 h, the number of CFUs was determined, which allowed the quantification of viable bacteria present on the inoculated solution. Five independent assays were performed, and bacterial cells incubated only with NB were used as a control.

Biofilm Inhibition Test. The quantification of biofilm total biomass, growing over the materials, was evaluated using crystal violet assay. For optimal biofilm growth, a concentration of 5×10^6 CFU·mL^{-1} *E. coli* inoculum was grown above the sterilized films on 24-well nontreated polystyrene plates for 24 h at 37 °C. Then, the medium was discarded, and biofilms washed with sterile PBS. This process was repeated three times to exclude non-adhered bacteria. Biofilms were further fixed using heat (60 °C) for 60 min. A solution of crystal violet at 0.1% (w/v) in PBS was placed in contact with the material and incubated for 10 min at RT. Crystal violet was removed, and samples were cleaned with distilled water three times. The residual stain was diluted with 30% acetic acid and a microplate reader (Biotek Cytation3) was used to measure the absorbance at 595 nm. PVDF 1010 films were used as a control sample, where cells adhered at certain extent and formed a biofilm.

Live/Dead Kit. The bacteria growing on the materials were further visualized under a fluorescence microscope after live/dead staining using a LIVE/DEAD BacLight Bacterial Viability Kit for microscopy (Invitrogen, US). *E. coli* was grown for 24 h on 24-well nontreated polystyrene plates over the sterilized films at 37 °C. Then, the samples were washed twice with PBS. The adhered cells were stained in dark conditions for 15 min with 0.1% (v/v) SYTO9 and 0.1% (v/v) propidium iodide. The samples were then visualized in a fluorescence microscope (Olympus BX51 microscope), and the obtained fields were captured using a magnification of 40X.

RESULTS AND DISCUSSION

Chemical Analysis of Nanodiamond Fillers. Figure 1 shows the XPS results of the ND samples. The C1s peak around 286 eV (Figure 1a,d,g,j) is assigned to sp^3 bonded carbon (C−C) and the peak at ≈284.6 eV refers to sp^2 carbons (C═C) associated to specific defects in the surface of the NDs.[34] The peaks at around 287 eV (C−O) and 288 eV (C═O) deal with ND oxygenated surface groups.

The O1s spectra (Figure 1b,e,h,k) were deconvoluted in three peaks attributed to C═O (529 eV), C−O (1) in ether, alcohol, and epoxy groups (530 eV), and C−O (2) in ester and carboxyl groups (532 eV). The oxygen content on the surface of the samples followed the order NDO > NDM > NDA > NDH, with the NDO sample (carboxylated) showing the highest oxygen content (9.5%), as expected, due to several oxygenated groups, as previously reported for samples thermally oxidized in air.[35] Non-functionalized ND (NDM) also showed a high oxygen content (6.3%) as a result of its production and purification procedures,[36] i.e., detonation with the explosive precursors 1,3,5-trinitroperhydro-1,3,5-triazine and 2,4,6-trinitrotoluene followed by a treatment with boiling acid to remove the impurities and the amorphous carbon resulting from the soot of detonation. The XPS results show that the treatments for hydrogenation and amination to obtain NDH and NDA materials resulted in the removal of most of the oxygenated groups from the surface, thereby reducing the oxygen concentration to about 2%.

The XPS profiles differ in the quantity of oxygenated groups in the surface and of sp^2 carbon. The lowest ratio of sp^2/sp^3 was registered in the non-functionalized NDM material (0.94), which shows that the functionalization treatments lead to an increase in the number of surface structural defects of ND.

The N1s XPS spectra of the ND samples (Figure 1c,f,i,l) can be deconvoluted in four components: the peak N6 is assigned to pyridinic-N groups (≈399 eV), the peak N5 corresponds to pyrrolic-N groups (≈400 eV), and the peak NQ deals with quaternary nitrogen (≈401);[37] the peaks at ≈403 and ≈405 eV are linked to N oxides.[38] The N content of the samples differed from 1.5% to 2.1%, characteristic of NDs obtained by detonation.[39−41] Nitrogen was present in the initial explosive mixture used to produce the NDs and was therefore likely incorporated into the diamond lattice.[36,42]

Morphology and Topography. The distribution of the NDs within the PVDF sample and the morphology of the composites were studied by SEM (Figure 2). Given the results similarity observed through SEM micrographs, only representative images are shown.

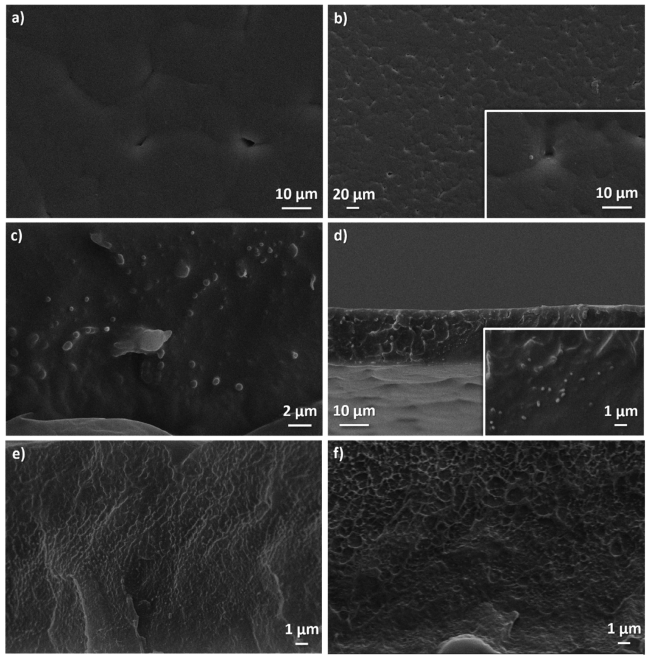

Figure 2. SEM micrographs of the surface of (a) NDH 0.5 wt %, (b) NDM 2 wt %, and the cross section of (c) NDO 0.5 wt %, (d) NDA 2 wt %, (e) NDH 0.25 wt %, and (f) NDM 2 wt %.

Figures 2a and b show the surface of the composites NDH and NDM, respectively, which is mostly regular and homogeneous throughout its extension and with the characteristic PVDF spherulitic structure. It is notorious that small pores are present between the spherulites, which resulted from high temperatures (210 °C) during the polymer processing.[43] In the inset of Figure 2b, it is possible to observe a ND aggregate near to the pore. The cross sections of the samples NDO 0.5 wt %, NDA 2 wt %, NDH 0.25 wt %, and NDM 2 wt % are presented in Figures 2c to f, respectively. All ND filler types appear well distributed and scattered along the section of the PVDF sample, also presenting homogeneous sizes in a submicron range. However, it is possible to identify some ND clusters of larger size in both the NDO and NDA samples, being more visible in the NDO sample, indicating that ND nanofillers with

https://dx.doi.org/10.1021/acsapm.0c00869
ACS Appl. Polym. Mater. 2020, 2, 5014−5024

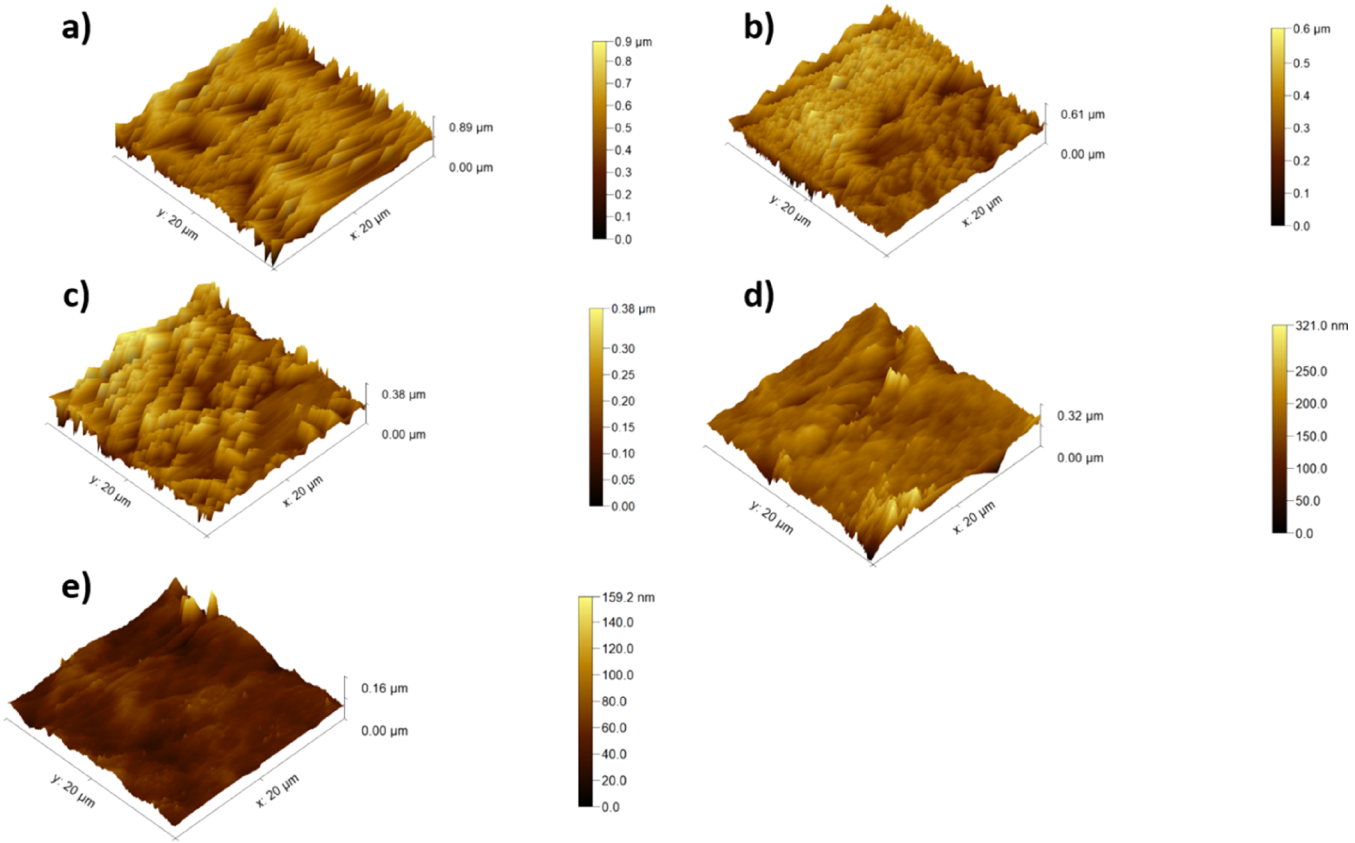

Figure 3. 3D AFM images of PVDF (a) and composites with 2 wt % of nanofillers NDM (b), NDO (c), NDA (d), and NDH (e).

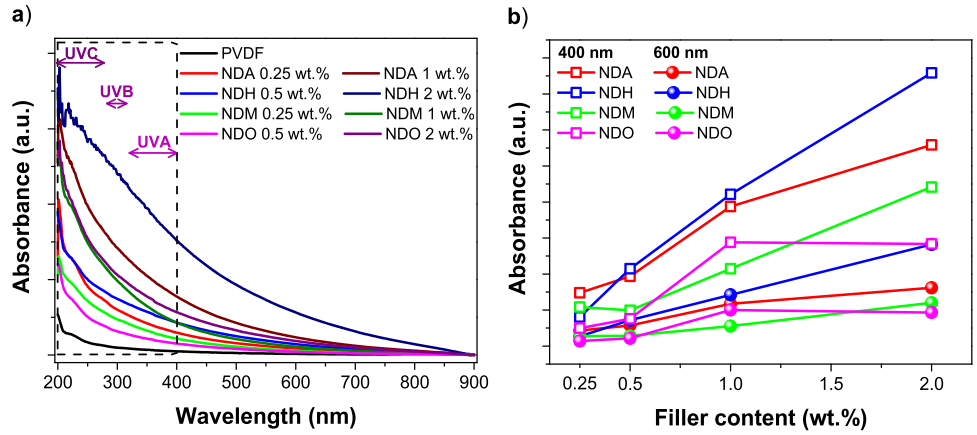

Figure 4. (a) UV−Vis absorbance spectra of pristine PVDF and various ND/PVDF composite films. (b) Optical absorbance as a function of ND content and type.

higher oxygen content are more difficult to disperse, similar to what was verified in a previous study.[12]

The topography of the samples was analyzed by AFM measurements for pristine PVDF and samples with 2 wt % of nanofiller content (Figure 3).

The analysis of Figure 3 shows that no relevant differences can be found between the overall topography of the PVDF sample and composites. The surface of the PVDF sample shows hills and valleys characteristic of the polymer film surface,[5] and this morphology is also present in the composite sample surface. A tendency for smaller ridges is observed compared to the pristine sample, indicating that the ND fillers contribute to a slight smoothing of the surface as a result of the interactions between the polymer and ND nanostructure. However, the addition of the ND nanofillers does not induce drastic changes in the roughness (Ra) of the samples, which present variations of Ra ranging between ≈10 and 100 nm for the NDH 2 wt % and PVDF, respectively.

The effect of the ND nanofillers in the wettability of the composites was evaluated by water contact angle, and the results are presented in Figure S1. It can be seen that water contact angle is not significantly influenced by the different types of NDs in the polymer matrix since all of them present similar values of approximately 81° for the materials with 0.25 wt %. This was expected since AFM measurements also showed similar topography and roughness among the samples.

https://dx.doi.org/10.1021/acsapm.0c00869
ACS Appl. Polym. Mater. 2020, 2, 5014−5024

Nevertheless, by increasing the content of filler from 0.25% to 2%, the wettability is increased. While pristine PVDF presents a contact angle of approximately 84°, the inclusion of the NDs decreases the contact angle to values below 80°. In general, the greater the surface roughness, the smaller the water contact angle.[44] The inclusion of the particles induces an even more uneven surface, thus increasing wettability.

Optical, Structural, and Thermal Properties. In Figure 4 are shown the UV−Vis spectra of the PVDF pristine polymer and ND/PVDF composites (Figure 4a) and the dependence of the absorbance of the nanocomposite films with ND filler concentration and type (Figure 4b).

By analyzing the UV−Vis spectra of the PVDF composite films with embedded NDA, NDH, NDM, and NDO between 200 and 800 nm (Figure 4a), it is verified that the ability of the nanocomposites in absorbing UV radiation increased with the presence and weight content of the ND fillers, being about 10 times higher for the NDH sample with 2 wt % than for the pristine PVDF in the UV region. This proves that ND particles have the ability to attenuate the transmission of UVA, UVB, and UVC radiation enabling their use as a UV filter.[45] In the near-infrared spectral region (750−800 nm), the nanocomposites were transparent, thus observing a general decrease in absorbance for almost all samples.[12,46] Figure 4b shows that the absorbance (at both the wavelengths of 400 and 600 nm) increased with increasing of the nanofiller concentration, regardless the ND type, presenting an increment of about 40% from 400 to 600 nm for the films with higher nanofiller concentration (2 wt %). The variations of the concentration and type of ND embedded into the PVDF films enable one to tune, to a certain extent, the optical properties of the composite samples in order to achieve specific application demands, specifically the absorption of UV radiation, which allows their use as components of sunscreens for UV radiation.[47] The films are near to transparent in the spectral regions of visible and near infrared and absorb in the UV region, providing effective protection from the UV radiation, and this behavior is similar to that reported for thin films of poly(vinylpyrrolidone) with NDs.[45]

Through FTIR-ATR spectroscopy, it was possible to identify the PVDF polymer phases and their relative content in the composites, which made it possible to reveal any effects of the nanofillers on the polymer crystallization. Figure 5 shows that all samples crystallized mainly in the non-polar α phase, with residual traces of the β phase. The exclusive and characteristic absorption bands of α-PVDF (766, 795, and 976 cm^{-1}) were found in the spectra, which was expected considering the selected processing conditions from the melt.[28] The α phase concentration, determined by eq 1, ranged between about 92% and 94% with the maximum value obtained for the sample with 0.5 wt % of NDO. Furthermore, no traces of γ-PVDF were detected. Thus, the addition of the ND fillers and the applied surface functionalizations did not interfere in the crystallization of PVDF and did not promote the nucleation of γ-PVDF, as observed in previous works with similar composites with ND[12] or with carbonaceous nanofillers.[48]

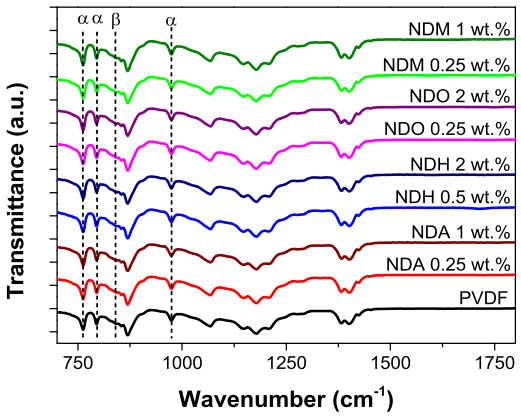

Figure 5. FTIR-ATR spectra of PVDF polymer and various ND/PVDF composites.

Figure S2 and Table T1 (Supporting Information) show representative thermograms and the corresponding sample crystallinity. The melting temperature (T_m) and the degree of crystallinity were determined from the DSC thermograms and eq 2, respectively. All the samples present the endothermic peak at approximately 170 °C (Figure S2, Supporting Information) ascribed to the melting of the α phase of the polymer,[28] which is in agreement with the α phase amounts mentioned above. No shifts were detected in the melting peak of the composites in comparison with the pristine PVDF film, with the exceptions of 2 wt % of NDM and 2 wt % of NDO films, which exhibited a shift of approximately +2 and −2 °C, respectively. In the case of 2 wt % of NDO, presumably larger interactions between ND nanofillers and the polymer matrix led to the enhancement of the composite thermal stability.[49] The degree of crystallinity (Table T1, Supporting Information) was determined through the enthalpy of the thermogram's melting peak, and the highest value (≈63%) was obtained for the PVDF film. Considering the experimental error of 3% in the calculation of the crystallinity, the differences in the degree of crystallinity were not significant (Table T1, Supporting Information). Nevertheless, it seems that the incorporation of the nanofillers to the polymer slightly reduces the degree of crystallinity, with a minimum of ≈58% in the case of 0.5 wt % NDA. This would suggest that the ND particles acted as defects during the crystallization process,[49] independently of the filler type or content.

Electrical Properties. Figure 6 shows the dielectric response (Figures 6a and b), a.c. (Figure 6c), and d.c. (Figure 6d) electrical conductivity.

Figure 6a shows a slight decrease in the dielectric constant (ε') with the increase in frequency (500 Hz to 1 MHz), typical of PVDF due to the dipolar relaxation characteristics of the polymer.[50] The presence of ND nanofillers did not change this dependence of ε' with the frequency; nonetheless, a general increase in ε' is observed for all composite films (7−9) compared to the pristine PVDF film (6−7), similar to that reported elsewhere for similar nanocomposites.[12] Nonetheless, no relation can be established between the increase in ε' and the type and content of the ND nanofillers, being most probably related to interfacial trapped charges and Maxwell−Wagner−Sillars relaxation,[51] which depend on the specific characteristics of the surfaces of the different ND functionalization types. The dielectric loss tangent ($\tan(\delta)$) in the range of 500 Hz to 1 MHz is presented in Figure 6b, showing a similar frequency dependence for all samples with a maximum value of $\tan(\delta)$ of approximately 0.1 at 1 MHz. It should be noted that the relative increase in ε' in the composites was not accompanied by an increase in the dielectric loss since pristine PVDF and the different composites all present similar $\tan(\delta)$ values, reinforcing the aforementioned behavior of the

https://dx.doi.org/10.1021/acsapm.0c00869
ACS Appl. Polym. Mater. 2020, 2, 5014−5024

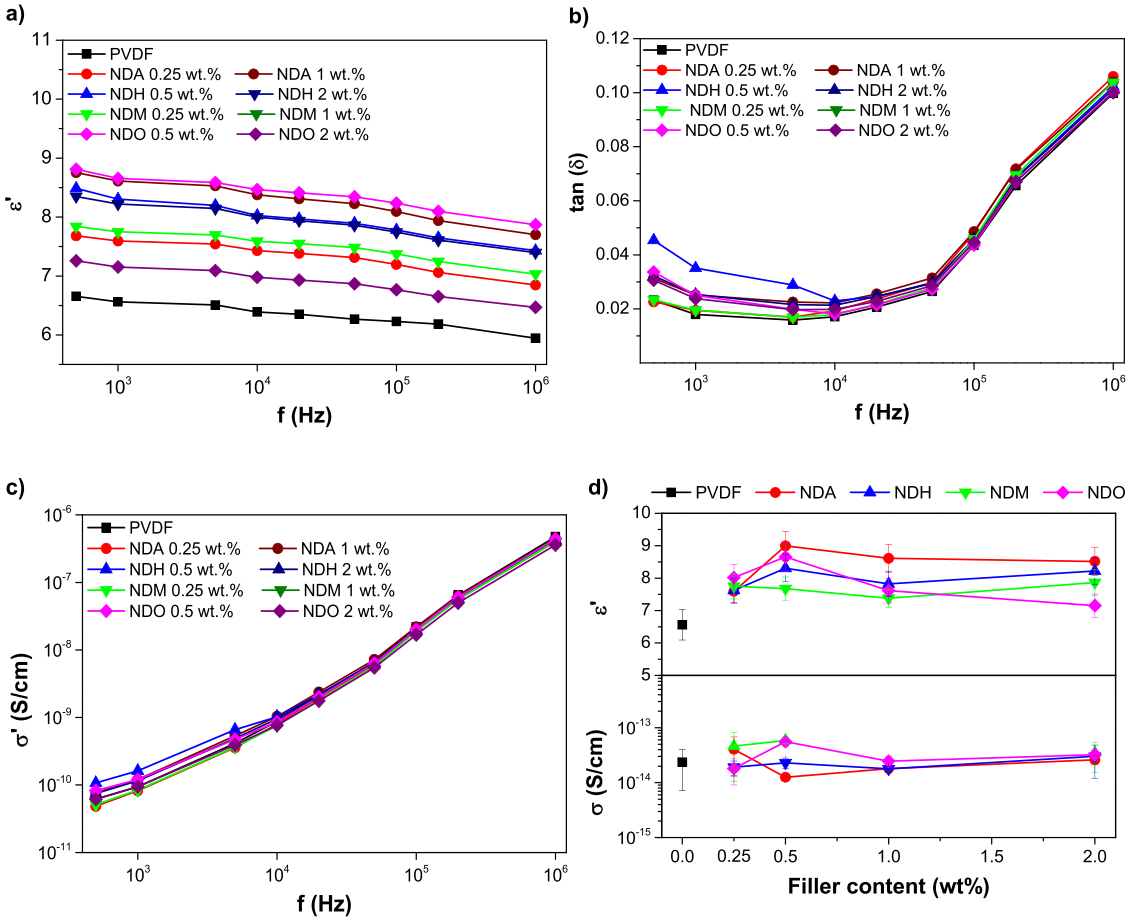

Figure 6. Electrical properties measured at room temperature: dielectric constant (a), dielectric loss (b), a.c. electrical conductivity as a function of frequency (c), dielectric constant (at 1 kHz), and d.c. conductivity as a function of filler content and type (d).

interfaces in the dielectric response. The overall behavior of the dielectric loss, in the referred frequency range, was similar for all samples, decreasing slightly up to 10^4 Hz and increasing markedly for frequencies above 10^5 Hz, typically attributed to the polymer α_a relaxation as well as to the contribution of localized charges and the crystallite/amorphous region interfaces.[52] The a.c. conductivity (σ') in Figure 6c increased with increasing frequency with no noticeable differences between composites and pristine PVDF films, meaning that the intrinsic nature of the PVDF sample was not modified.[53] The relation between ε' at 1 kHz and d.c. electrical conductivity (σ) with the nanofiller type and content is presented in Figure 6d. It is shown that ε' (Figure 6d, top) tends to increase with the incorporation of ND nanofillers, the pristine PVDF sample presenting $\varepsilon' \approx 6.5$ and the composite with 0.5 wt % of NDA displaying the maximum $\varepsilon' \approx 9$. An increase in ε' by approximately 1.5−2.5 was verified in the nanocomposite samples regardless the type and the concentration of ND, whereas little significant differences were found between them. The aminated sample showed relatively higher values among the composites, with the exception of the sample NDA 0.25 wt %. The σ of the composites (Figure 6d, bottom) did not change significantly with respect to that of the pristine PVDF film; the d.c. conductivity had the same order of magnitude (10^{-14} S/cm) for all samples and the differences were within experimental errors.

Antimicrobial and Antibiofilm Activity. *E. coli* is responsible for a high number of infections worldwide, from mild infections such as common urinary infections to serious ones like hemorrhagic colitis, responsible for many large-scale outbreaks in recent years.[54] The susceptibility of *E. coli* toward NDs was measured in culture media to assess the capability of these nanostructures alone, i.e., before being incorporated in the composite, for inhibiting the growth of bacteria. Increasing concentrations of NDs in suspension were then put in contact with *E. coli* overnight, and the optical density was measured after 24 h incubation, which is an indication of ND bacteriostatic activity. The determination of ND capability to inhibit bacterial growth comes from the knowledge that the nanoscaled material has the ability to interact with the membrane of the bacterial cell due to its larger surface area, inducing high local membrane perturbance, which eventually leads to cell leakage and thus death.[55,56] Figure 7 shows that amine-containing NDs (NDA) possessed higher ability to prevent the *E. coli* growth followed by the hydrogenated (NDH) and carboxylated (NDO) variants. However, non-functionalized NDs (NDM) showed no bacteriostatic activity, evidenced by a linear OD with increasing concentration, which means that NDM did not affect the susceptibility of bacteria. The surficial functional groups of the NDs thus play an essential role on the antimicrobial activity of these structures. As expected, the NDs comprising amino groups, thus providing a cationic nature to the structures, are the ones with higher antimicrobial activity. It has been widely proven that cationic nanostructures are able to effectively induce bacterial cell damage.[55,57]

https://dx.doi.org/10.1021/acsapm.0c00869
ACS Appl. Polym. Mater. 2020, 2, 5014−5024

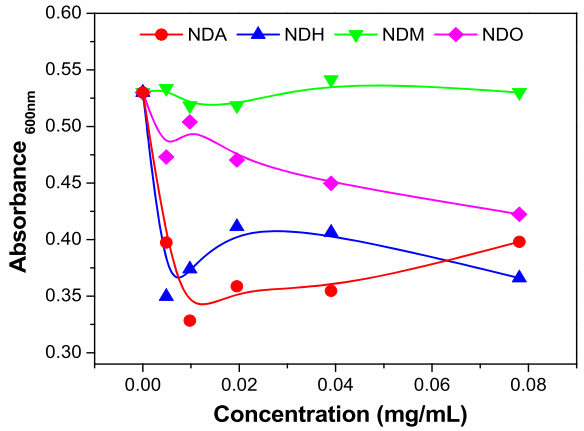

Figure 7. Dose-dependent effect of the non-functionalized and functionalized NDs in the inhibition of *E. coli* growth, measured after overnight contact with bacteria at OD at 600 nm.

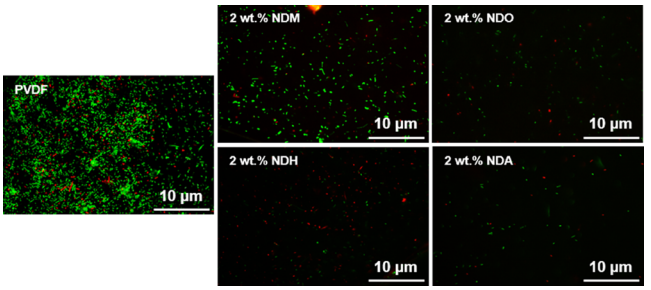

Figure 9. Fluorescence microscopy live/dead images of 24 h grown *E. coli* bacteria incubated over the nanocomposites and PVDF as a control (live cells in green and dead cells in red).

Despite the fact that most of the NDs in suspension show antibacterial activity, the incorporation into the PVDF matrix may narrow the interaction with bacteria and the antimicrobial effect. Therefore, the corresponding PVDF composites were further tested for their antimicrobial activity. The nanocomposites comprising the highest concentration of NDs (2 wt %) were chosen to study the effect of the addition of ND structures to the films, not losing focus on the influence of polymer's morphology on the interaction with bacteria.

The tests were performed both at the surface of the materials through the evaluation of the total biomass and bacteria adhered to their surfaces as well as by studying the capability to induce a killing effect on the bacteria in suspension over the material. It was observed that the antimicrobial properties of the film materials were mainly confined to the surface since no CFU reduction in suspension was observed. These results are presented in Figures 8 and 9. In Figure 8a, it can be observed that the amount of *E. coli* in solution was not affected since no relevant differences were found in terms of log reduction. This indicates that the material itself was not antimicrobial or did not leach the ND filler into the solution, which could induce bacterial death.

Nevertheless, by observing the surface of the material, analyzed with crystal violet assay (Figure 8b) and live/dead kit (Figure 9), all the nanocomposites inhibited, to a different extent, the formation of biofilm when compared to the PVDF film without any ND. The inclusion of nanodiamonds on the material surface thus influenced the capability of bacteria to adhere and form the biofilm. This is in line with previous studies that demonstrated that some specific nanostructured surfaces such as ridges, nanopillars, and grooves are able to avoid the bacteria adhesion and inhibit biofilm formation.[58,59] Since the herein developed materials present a very similar topography (Figures 2 and 3), it is proposed that the antimicrobial activity of the films is due to the NDs themselves, which act by contact killing due to their nanosized structure.

Figure 9 clearly shows that the *E. coli* cells adhered to the PVDF surface, most of the cells staining green, indicating a high level of bacterial viability and to a lesser extent to the NDM nanocomposite material, which presents a relatively higher cell density among the ND/PVDF composites. On the other composite materials, besides having less cell density on the surface, they were mainly dead (represented in red), with the highest number of dead cells found over the NDH and NDA containing composites. These results corroborate with the results shown in Figure 7 where these functionalized NDs were found to induce more bacteriostatic activity.

With respect to the possible mechanism of action of the NDs, it can be hypothesized that NDs are able to kill bacteria through contact killing mechanism via the interaction with nanosized clusters that disrupt the cell membrane. It has been reported that specific nanostructures, mainly positively charged ones, have the ability to interact with the bacterial cell membrane due to their larger surface area, inducing high local membrane perturbance, which eventually leads to cell leakage and thus death.[55,60] In fact, cationic biocides and surfactants (e.g., quaternary ammonium compounds), both possessing

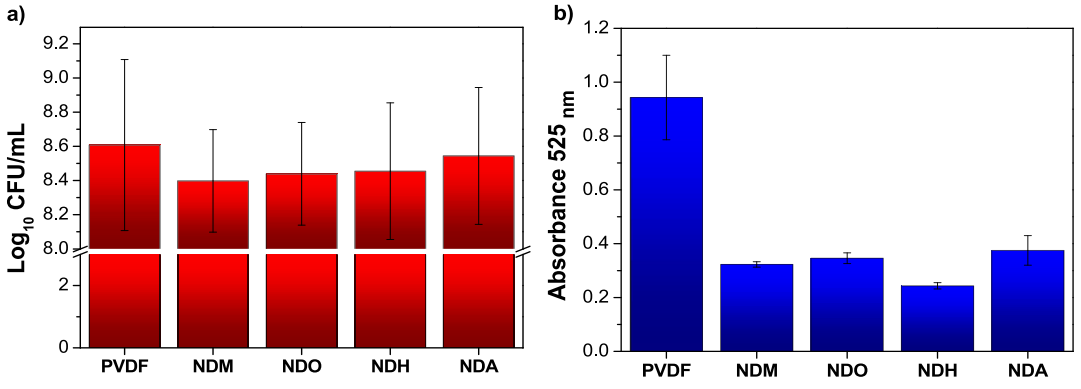

Figure 8. Antimicrobial activity of the pristine PVDF and ND/PVDF films (2 wt %) measured using (a) CFUs (colony-forming units) of *E. coli* growing in suspension over the nanocomposites and (b) the total biomass growing on material's surface assessed by crystal violet assay.

https://dx.doi.org/10.1021/acsapm.0c00869
ACS Appl. Polym. Mater. 2020, 2, 5014−5024

positively charged moieties, were reported to impart bactericidal properties for a wide range of bacteria.[61,62]

It could thus be concluded that these NDs acted by contact killing and were not leached from the material. Thus, the developed composites can be used as antimicrobial coatings, being the NDA and NDH enriched composites particularly suitable for this application. Moreover, the polymer matrix enables green chemistry approaches[63] during processing, including additive manufacturing technologies.[64]

CONCLUSIONS

ND/PVDF composites were processed by solvent casting using ND fillers of four different types of surface functionalization (i.e., non-functionalized (NDM), aminated (NDA), hydrogenated (NDH), and carboxylated (NDO)) and concentrations (0.25, 0.5, 1, and 2 wt %).

The samples showed homogeneous surface morphology and regular dispersion of ND fillers across the PVDF sample for all composites, while the overall surface topography was similar between the composites and pristine PVDF sample. The contact angle was therefore very similar among the samples, slightly increasing with the increase in ND concentration in the PVDF matrix.

As compared to the pristine PVDF film, composite films showed up to 10 times higher absorbance in the UV region and about 40% higher absorbance in the visual light region (i.e., at 400 and 600 nm) in the case of the NDH sample 2 wt %. All films crystallized in the α-PVDF phase (92−94%), with smaller traces of β-PVDF, so the filler type or filler content did not affect the α phase crystallization of PVDF. The dielectric constant (ε') of the composite films increased with about 2 with the incorporation of ND, and the dielectric loss ($\tan(\delta)$) remained almost constant. The inclusion of ND imparted antibiofilm properties to the films, with the type of ND functionalization being an essential factor to kill the bacterial cells through contact killing. NDH and NDA containing composites induced improved bactericidal activity when compared to NDM and NDO, most probably due to the effective interaction with the membrane of the bacterial cell. In short, the incorporation of several ND fillers into PVDF enables one to tune the optical properties of the nanocomposites, increases the dielectric constant while not affecting the dielectric loss, and successfully imparts antimicrobial properties to the films without relevant modification of the characteristics of PVDF. These composites represent promising candidates to produce functional coatings and sensors due to the outstanding properties of the polymer, including through additive manufacturing processes.

ASSOCIATED CONTENT

Supporting Information

The Supporting Information is available free of charge at https://pubs.acs.org/doi/10.1021/acsapm.0c00869.

Water contact angle (Figure S1), DSC thermograms (Figure S2), and degree of crystallinity (Table T1) (PDF)

AUTHOR INFORMATION

Corresponding Authors

João Nunes-Pereira − *Centre for Mechanical and Aerospace Science and Technologies (C-MAST), Universidade da Beira Interior, 6200-001 Covilhã, Portugal; Centro de Física das Universidades do Minho e do Porto (CF-UM-UP), 4710-057 Braga, Portugal;* orcid.org/0000-0002-6024-8716; Email: j.nunespereira@ubi.pt

Senentxu Lanceros-Mendez − *BCMaterials, Basque Center for Materials, Applications and Nanostructures, 48940 Leioa, Spain; IKERBASQUE, Basque Foundation for Science, 48009 Bilbao, Spain*; Email: senentxu.lanceros@bcmaterials.net

Authors

Pedro Costa − *Centro de Física das Universidades do Minho e do Porto (CF-UM-UP), 4710-057 Braga, Portugal; Institute for Polymers and Composites IPC/I3N, University of Minho, 4800-058 Guimarães, Portugal;* orcid.org/0000-0001-9887-0925

Liliana Fernandes − *Centro de Física das Universidades do Minho e do Porto (CF-UM-UP), 4710-057 Braga, Portugal*

Estela O. Carvalho − *Centro de Física das Universidades do Minho e do Porto (CF-UM-UP), 4710-057 Braga, Portugal; Centre of Biological Engineering, University of Minho, 4710-057 Braga, Portugal*

Margarida M. Fernandes − *Centro de Física das Universidades do Minho e do Porto (CF-UM-UP), 4710-057 Braga, Portugal; Centre of Biological Engineering, University of Minho, 4710-057 Braga, Portugal;* orcid.org/0000-0002-1529-3702

Sónia A. C. Carabineiro − *LAQV-REQUIMTE, Department of Chemistry, NOVA School of Science and Technology, Universidade NOVA de Lisboa, 2829-516 Caparica, Portugal*

Josephus G. Buijnsters − *Department of Precision and Microsystems Engineering, Micro and Nano Engineering, Delft University of Technology, 2628 CD Delft, The Netherlands*

Carmen R. Tubio − *BCMaterials, Basque Center for Materials, Applications and Nanostructures, 48940 Leioa, Spain;* orcid.org/0000-0002-6988-8242

Complete contact information is available at: https://pubs.acs.org/10.1021/acsapm.0c00869

Author Contributions

The manuscript was written through contributions of all authors. All authors have given approval to the final version of the manuscript.

Notes

The authors declare no competing financial interest.

ACKNOWLEDGMENTS

The authors thank the Fundação para a Ciência e a Tecnoloiga (FCT), Fundo Social Europeu (FSE) and Programa Operacional Regional Centro 2020, Norte 2020 and Lisboa 2020 for the Strategic Funding UID/EMS/00151/2020 and UID/FIS/04650/2020, projects PTDC/BTM-MAT/28237/2017 and PTDC/EMD-EMD/28159/2017, and the grants SFRH/BPD/117838/2016 (J.N.P.), SFRH/BPD/110914/2015 (P.C.), SFRH/BD/145345/2019 (L.F.), SFRH/BD/145455/2019 (E.O.C.), SFRH/BPD/121464/2016 (M.M.F.) and Associate Laboratory for Green Chemistry—LAQV, which is financed by national funds from FCT/MCTES (UIDB/50006/2020). J.G.B. thanks the Dutch Research Council (NWO) for funding as part of the Open Technology Programme (project no. 16361). Financial support from the Spanish State Research Agency (AEI) and the European Regional Development Fund (ERFD) through the project PID2019-106099RB-C43/AEI/10.13039/501100011033 and

from the Basque Government Industry and Education Departments under the ELKARTEK, HAZITEK and PIBA (PIBA-2018-06) programs is also acknowledged. The authors thank Dr. Carlos Sá (CEMUP) for assistance with the XPS analyses.

■ ABBREVIATIONS

ATCC, American Type Culture Collection; AFM, atomic force microscopy; ATR, attenuated total reflectance; BE, binding energy; CFU, colony-forming units; DCS, differential scanning calorimetry; DMF, *N*,*N*-dimethylformamide; *E. coli*, *Escherichia coli*; FAT, fixed analyzer transmission; FTIR, Fourier transform infrared spectroscopy; NB, Nutrient Broth; NDA, uDiamond Amine (Carbodeon); NDH, uDiamond Hydrogen P (Carbodeon); NDM, uDiamond Molto (Carbodeon); NDO, uDiamond Vox P (Carbodeon); NDPC, phospholipid ND compound; NDs, nanodiamonds; OD, optical density; PBS, phosphate buffer solution; PLGA, poly(lactic-*co*-glycolic acid); PVDF, poly(vinylidene fluoride); SD, standard deviation; SEM, scanning electron microscopy; XPS, X-ray photoelectron spectroscopy

■ REFERENCES

(1) Yu, J.; Qian, R.; Jiang, P. Enhanced thermal conductivity for PVDF composites with a hybrid functionalized graphene sheet-nanodiamond filler. *Fibers Polym.* **2013**, *14*, 1317−1323.
(2) Prasad, K. E.; Das, B.; Maitra, U.; Ramamurty, U.; Rao, C. N. R. Extraordinary synergy in the mechanical properties of polymer matrix composites reinforced with 2 nanocarbons. *Proc. Natl. Acad. Sci.* **2009**, *106*, 13186−13189.
(3) Martins, P.; Nunes, J. S.; Oliveira, J.; Perinka, N.; Lanceros-Mendez, S. Spray-printed magnetoelectric multifunctional composites. *Composites, Part B* **2020**, *187*, 107829.
(4) Li, E.; Ye, P.; Kang, J.; Yin, C.; Cheng, F. Facile fabrication of photochromic microspheres with multimodal hierarchically porous for selective extraction of lithium ions. *Mater. Lett.* **2020**, *270*, 127670.
(5) Correia, D. M.; Nunes-Pereira, J.; Alikin, D.; Kholkin, A. L.; Carabineiro, S. A. C.; Rebouta, L.; Rodrigues, M. S.; Vaz, F.; Costa, C. M.; Lanceros-Méndez, S. Surface wettability modification of poly(vinylidene fluoride) and copolymer films and membranes by plasma treatment. *Polymer* **2019**, *169*, 138−147.
(6) Zhang, Z.-Q.; Zeng, R.-C.; Lin, C.-G.; Wang, L.; Chen, X.-B.; Chen, D.-C. Corrosion resistance of self-cleaning silane/polypropylene composite coatings on magnesium alloy AZ31. *J. Mater. Sci. Technol.* **2020**, *41*, 43−55.
(7) Ojogbo, E.; Ward, V.; Mekonnen, T. H. Functionalized starch microparticles for contact-active antimicrobial polymer surfaces. *Carbohydr. Polym.* **2020**, *229*, 115422.
(8) Mochalin, V. N.; Shenderova, O.; Ho, D.; Gogotsi, Y. The properties and applications of nanodiamonds. *Nat. Nanotechnol.* **2012**, *7*, 11−23.
(9) Meinhardt, T.; Lang, D.; Dill, H.; Krueger, A. Pushing the functionality of diamond nanoparticles to new horizons: Orthogonally functionalized nanodiamond using click chemistry. *Adv. Funct. Mater.* **2011**, *21*, 494−500.
(10) Zhang, Y.; Choi, J. R.; Park, S.-J. Thermal conductivity and thermo-physical properties of nanodiamond-attached exfoliated hexagonal boron nitride/epoxy nanocomposites for microelectronics. *Composites, Part A* **2017**, *101*, 227−236.
(11) Zhang, Y.; Rhee, K. Y.; Hui, D.; Park, S.-J. A critical review of nanodiamond based nanocomposites: Synthesis, properties and applications. *Composites, Part B* **2018**, *143*, 19−27.
(12) Nunes-Pereira, J.; Silva, A. R.; Ribeiro, C.; Carabineiro, S. A. C.; Buijnsters, J. G.; Lanceros-Méndez, S. Nanodiamonds/poly(vinylidene fluoride) composites for tissue engineering applications. *Composites, Part B* **2017**, *111*, 37−44.
(13) Al-Jumaili, A.; Alancherry, S.; Bazaka, K.; Jacob, M. V. Review on the antimicrobial properties of carbon nanostructures. *Materials* **2017**, *10*, 1066.
(14) Szunerits, S.; Barras, A.; Boukherroub, R. Antibacterial applications of nanodiamonds. *Int. J. Environ. Res. Public Health* **2016**, *13*, 413−413.
(15) Wilks, S. A.; Michels, H.; Keevil, C. W. The survival of *Escherichia coli* O157 on a range of metal surfaces. *Int. J. Food Microbiol.* **2005**, *105*, 445−454.
(16) Liau, S. Y.; Read, D. C.; Pugh, W. J.; Furr, J. R.; Russell, A. D. Interaction of silver nitrate with readily identifiable groups: relationship to the antibacterialaction of silver ions. *Lett. Appl. Microbiol.* **2003**, *25*, 279−283.
(17) Ioannou, C. J.; Hanlon, G. W.; Denyer, S. P. Action of disinfectant quaternary ammonium compounds against staphylococcus aureus. *Antimicrob. Agents Chemother.* **2006**, *51*, 296−306.
(18) Mao, B.-H.; Chen, Z.-Y.; Wang, Y.-J.; Yan, S.-J. Silver nanoparticles have lethal and sublethal adverse effects on development and longevity by inducing ROS-mediated stress responses. *Sci. Rep.* **2018**, *8*, 2445.
(19) Bumgardner, J. D.; Lucas, L. C.; Tilden, A. B. Toxicity of copper-based dental alloys in cell culture. *J. Biomed. Mater. Res.* **1989**, *23*, 1103−1114.
(20) Fouda, S. M.; Gad, M. M.; Ellakany, P.; Al-Thobity, A. M.; Al-Harbi, F. A.; Virtanen, J. I.; Raustia, A. The effect of nanodiamonds on candida albicans adhesion and surface characteristics of PMMA denture base material - an in vitro study. *J. Appl. Oral Sci.* **2019**, *27*, No. e20180779.
(21) Chen, M.; Pierstorff, E. D.; Lam, R.; Li, S.-Y.; Huang, H.; Osawa, E.; Ho, D. Nanodiamond-mediated delivery of water-insoluble therapeutics. *ACS Nano* **2009**, *3*, 2016−2022.
(22) Lim, D. G.; Jung, J. H.; Ko, H. W.; Kang, E.; Jeong, S. H. Paclitaxel−nanodiamond nanocomplexes enhance aqueous dispersibility and drug retention in cells. *ACS Appl. Mater. Interfaces* **2016**, *8*, 23558−23567.
(23) Giammarco, J.; Mochalin, V. N.; Haeckel, J.; Gogotsi, Y. The adsorption of tetracycline and vancomycin onto nanodiamond with controlled release. *J. Colloid Interface Sci.* **2016**, *468*, 253−261.
(24) Toh, T.-B.; Lee, D.-K.; Hou, W.; Abdullah, L. N.; Nguyen, J.; Ho, D.; Chow, E. K.-H. Nanodiamond−mitoxantrone complexes enhance drug retention in chemoresistant breast cancer cells. *Mol. Pharmaceutics* **2014**, *11*, 2683−2691.
(25) Zhang, F.; Song, Q.; Huang, X.; Li, F.; Wang, K.; Tang, Y.; Hou, C.; Shen, H. A novel high mechanical property PLGA composite matrix loaded with nanodiamond−phospholipid compound for bone tissue engineering. *ACS Appl. Mater. Interfaces* **2016**, *8*, 1087−1097.
(26) Simioni, N. B.; Silva, T. A.; Oliveira, G. G.; Fatibello-Filho, O. A nanodiamond-based electrochemical sensor for the determination of pyrazinamide antibiotic. *Sens. Actuators, B* **2017**, *250*, 315−323.
(27) Schrand, A. M.; Hens, S. A. C.; Shenderova, O. A. Nanodiamond particles: properties and perspectives for bioapplications. *Crit. Rev. Solid State Mater. Sci.* **2009**, *34*, 18−74.
(28) Martins, P.; Lopes, A. C.; Lanceros-Mendez, S. Electroactive phases of poly(vinylidene fluoride): Determination, processing and applications. *Prog. Polym. Sci.* **2014**, *39*, 683−706.
(29) Ribeiro, C.; Costa, C. M.; Correia, D. M.; Nunes-Pereira, J.; Oliveira, J.; Martins, P.; Gonçalves, R.; Cardoso, V. F.; Lanceros-Méndez, S. Electroactive poly(vinylidene fluoride)-based structures for advanced applications. *Nat. Protoc.* **2018**, *13*, 681−704.
(30) Carvalho, E. O.; Fernandes, M. M.; Padrao, J.; Nicolau, A.; Marqués-Marchán, J.; Asenjo, A.; Gama, F. M.; Ribeiro, C.; Lanceros-Mendez, S. Tailoring bacteria response by piezoelectric stimulation. *ACS Appl. Mater. Interfaces* **2019**, *11*, 27297−27305.
(31) Mendes-Felipe, C.; Oliveira, J.; Etxebarria, I.; Vilas-Vilela, J. L.; Lanceros-Mendez, S. State-of-the-art and future challenges of UV curable polymer-based smart materials for printing technologies. *Adv. Mater. Technol.* **2019**, *4*, 1800618.

https://dx.doi.org/10.1021/acsapm.0c00869
ACS Appl. Polym. Mater. 2020, 2, 5014−5024

(32) Fu, Y.; Yang, Q.; Xu, M.; Kong, H.; Chen, H.; Fu, Y.; Yao, Y.; Zhou, H.; Zhou, J. Secondary bacterial infections in critical ill patients with coronavirus disease 2019. *Open Forum Infect. Dis.* **2020**, *7*, ofaa220.
(33) Benz, M.; Euler, W. B. Determination of the crystalline phases of poly(vinylidene fluoride) under different preparation conditions using differential scanning calorimetry and infrared spectroscopy. *J. Appl. Polym. Sci.* **2003**, *89*, 1093−1100.
(34) Holt, K. B.; Caruana, D. J.; Millán-Barrios, E. J. Electrochemistry of undoped diamond nanoparticles: Accessing surface redox states. *J. Am. Chem. Soc.* **2009**, *131*, 11272−11273.
(35) Pastrana-Martínez, L. M.; Morales-Torres, S.; Carabineiro, S. A. C.; Buijnsters, J. G.; Faria, J. L.; Figueiredo, J. L.; Silva, A. M. T. Nanodiamond-TiO_2 composites for heterogeneous photocatalysis. *ChemPlusChem* **2013**, *78*, 801−807.
(36) Dolmatov, V. Y. Detonation-synthesis nanodiamonds: synthesis, structure, properties and applications. *Russ. Chem. Rev.* **2007**, *76*, 339.
(37) Jansen, R. J. J.; van Bekkum, H. XPS of nitrogen-containing functional groups on activated carbon. *Carbon* **1995**, *33*, 1021−1027.
(38) Duan, X.; Ao, Z.; Li, D.; Sun, H.; Zhou, L.; Suvorova, A.; Saunders, M.; Wang, G.; Wang, S. Surface-tailored nanodiamonds as excellent metal-free catalysts for organic oxidation. *Carbon* **2016**, *103*, 404−411.
(39) Jiang, T.; Xu, K. FTIR study of ultradispersed diamond powder synthesized by explosive detonation. *Carbon* **1995**, *33*, 1663−1671.
(40) Kuznetsov, V. L.; Aleksandrov, M. N.; Zagoruiko, I. V.; Chuvilin, A. L.; Moroz, E. M.; Kolomiichuk, V. N.; Likholobov, V. A.; Brylyakov, P. M.; Sakovitch, G. V. Study of ultradispersed diamond powders obtained using explosion energy. *Carbon* **1991**, *29*, 665−668.
(41) Mironov, E.; Koretz, A.; Petrov, E. Detonation synthesis ultradispersed diamond structural properties investigation by infrared absorption. *Diamond Relat. Mater.* **2002**, *11*, 872−876.
(42) Kirmani, A. R.; Peng, W.; Mahfouz, R.; Amassian, A.; Losovyj, Y.; Idriss, H.; Katsiev, K. On the relation between chemical composition and optical properties of detonation nanodiamonds. *Carbon* **2015**, *94*, 79−84.
(43) Mendes, S. F.; Costa, C. M.; Caparros, C.; Sencadas, V.; Lanceros-Méndez, S. Effect of filler size and concentration on the structure and properties of poly(vinylidene fluoride)/$BaTiO_3$ nanocomposites. *J. Mater. Sci.* **2012**, *47*, 1378−1388.
(44) Prajitno, D. H.; Maulana, A.; Syarif, D. G. Effect of surface roughness on contact angle measurement of nanofluid on surface of stainless steel 304 by sessile drop method. *J. Phys.: Conf. Ser.* **2016**, *739*, No. 012029.
(45) Attia, N. F.; Rao, J. P.; Geckeler, K. E. Nanodiamond−polymer nanoparticle composites and their thin films. *J. Nanopart. Res.* **2014**, *16*, 2361.
(46) Papagiannouli, I.; Bourlinos, A. B.; Bakandritsos, A.; Couris, S. Nonlinear optical properties of colloidal carbon nanoparticles: nanodiamonds and carbon dots. *RSC Adv.* **2014**, *4*, 40152−40160.
(47) Wu, M.-S.; Sun, D.-S.; Lin, Y.-C.; Cheng, C.-L.; Hung, S.-C.; Chen, P.-K.; Yang, J.-H.; Chang, H.-H. Nanodiamonds protect skin from ultraviolet B-induced damage in mice. *J. Nanobiotechnol.* **2015**, *13*, 35.
(48) Nunes-Pereira, J.; Sharma, P.; Fernandes, L. C.; Oliveira, J.; Moreira, J. A.; Sharma, R. K.; Lanceros-Mendez, S. Poly(vinylidene fluoride) composites with carbon nanotubes decorated with metal nanoparticles. *Composites, Part B* **2018**, *142*, 1−8.
(49) Martins, P.; Costa, C. M.; Lanceros-Mendez, S. Nucleation of electroactive β-phase poly(vinilidene fluoride) with $CoFe_2O_4$ and $NiFe_2O_4$ nanofillers: a new method for the preparation of multiferroic nanocomposites. *Appl. Phys. A* **2011**, *103*, 233−237.
(50) Sousa, R. E.; Nunes-Pereira, J.; Ferreira, J. C. C.; Costa, C. M.; Machado, A. V.; Silva, M. M.; Lanceros-Mendez, S. Microstructural variations of poly(vinylidene fluoride co-hexafluoropropylene) and their influence on the thermal, dielectric and piezoelectric properties. *Polym. Test.* **2014**, *40*, 245−255.
(51) Lopes, A. C.; Costa, C. M.; Serra, R. S. i.; Neves, I. C.; Ribelles, J. L. G.; Lanceros-Méndez, S. Dielectric relaxation, ac conductivity and electric modulus in poly(vinylidene fluoride)/NaY zeolite composites. *Solid State Ionics* **2013**, *235*, 42−50.
(52) Sasabe, H.; Saito, S.; Asahina, M.; Kakutani, H. Dielectric relaxations in poly(vinylidene fluoride). *J. Polym. Sci., Polym. Phys.* **1969**, *7*, 1405−1414.
(53) Carabineiro, S. A. C.; Thavorn-Amornsri, T.; Pereira, M. F. R.; Serp, P.; Figueiredo, J. L. Comparison between activated carbon, carbon xerogel and carbon nanotubes for the adsorption of the antibiotic ciprofloxacin. *Catal. Today* **2012**, *186*, 29−34.
(54) Allocati, N.; Masulli, M.; Alexeyev, M. F.; Di Ilio, C. *Escherichia coli* in Europe: an overview. *Int. J. Environ. Res. Public Health* **2013**, *10*, 6235−6254.
(55) Fernandes, M. M.; Francesko, A.; Torrent-Burgués, J.; Carrión-Fité, F. J.; Heinze, T.; Tzanov, T. Sonochemically processed cationic nanocapsules: Efficient antimicrobials with membrane disturbing capacity. *Biomacromolecules* **2014**, *15*, 1365−1374.
(56) Fernandes, M. M.; Ivanova, K.; Hoyo, J.; Pérez-Rafael, S.; Francesko, A.; Tzanov, T. Nanotransformation of vancomycin overcomes the intrinsic resistance of Gram-negative bacteria. *ACS Appl. Mater. Interfaces* **2017**, *9*, 15022−15030.
(57) Liu, L.; Xu, K.; Wang, H.; Jeremy Tan, P. K.; Fan, W.; Venkatraman, S. S.; Li, L.; Yang, Y.-Y. Self-assembled cationic peptide nanoparticles as an efficient antimicrobial agent. *Nat. Nanotechnol.* **2009**, *4*, 457−463.
(58) Hasan, J.; Crawford, R. J.; Ivanova, E. P. Antibacterial surfaces: The quest for a new generation of biomaterials. *Trends Biotechnol.* **2013**, *31*, 295.
(59) Hasan, J.; Chatterjee, K. Recent advances in engineering topography mediated antibacterial surfaces. *Nanoscale* **2015**, *7*, 15568−15575.
(60) Zhou, C.; Wang, F.; Chen, H.; Li, M.; Qiao, F.; Liu, Z.; Hou, Y.; Wu, C.; Fan, Y.; Liu, L.; Wang, S.; Wang, Y. Selective antimicrobial activities and action mechanism of micelles self-assembled by cationic oligomeric surfactants. *ACS Appl. Mater. Interfaces* **2016**, *8*, 4242−4249.
(61) Blesic, M.; Marques, M. H.; Plechkova, N. V.; Seddon, K. R.; Rebelo, L. P. N.; Lopes, A. Self-aggregation of ionic liquids: micelle formation in aqueous solution. *Green Chem.* **2007**, *9*, 481−490.
(62) Jungnickel, C.; Łuczak, J.; Ranke, J.; Fernández, J. F.; Müller, A.; Thöming, J. Micelle formation of imidazolium ionic liquids in aqueous solution. *Colloids Surf., A* **2008**, *316*, 278−284.
(63) Nunes-Pereira, J.; Martins, P.; Cardoso, V. F.; Costa, C. M.; Lanceros-Méndez, S. A green solvent strategy for the development of piezoelectric poly(vinylidene fluoride−trifluoroethylene) films for sensors and actuators applications. *Mater. Des.* **2016**, *104*, 183−189.
(64) Oliveira, J.; Correia, V.; Castro, H.; Martins, P.; Lanceros-Mendez, S. Polymer-based smart materials by printing technologies: Improving application and integration. *Addit. Manuf.* **2018**, *21*, 269−283.

https://dx.doi.org/10.1021/acsapm.0c00869
ACS Appl. Polym. Mater. 2020, 2, 5014−5024